Optimal Mass, Spin, and Orientation Parameters for Detecting Higher Order Gravitational-wave Modes from Binary Black Hole Mergers

Mahlet Shiferaw*
Harvard-Smithsonian Center for Astrophysics, Cambridge, MA 02138

Alan Weinstein† and Liting Xiao‡
LIGO, California Institute of Technology, Pasadena, CA 91125

(LIGO Collaboration)

(Dated: August 2, 2019)

Thus far, the Advanced Laser Interferometer Gravitational-Wave Observatory (aLIGO) and Advanced Virgo have detected gravitational waves (GWs), or ripples in the curvature of spacetime, from dozens of binary black hole (BBH) and binary neutron star (BNS) mergers. In order to detect the GWs from these mergers, aLIGO data are optimally searched using matched filtering against a bank of model waveform templates which are well-described by General Relativity (GR). Currently, such searches only utilize waveforms for the dominant Y_{22} mode, neglecting higher order modes (HOMs). However, these HOMs carry information about the source and the radiation it emits, and are therefore of great interest to study. Our goal is to identify the presence of HOMs in signals found in the data in order to test GR. Using a newly-released catalog of BBH simulations with HOMs developed by the Simulating eXtreme Spacetimes (SXS) Collaboration, we will assess the capabilities of aLIGO for detecting HOMs. Such detections are currently very unlikely, as HOMs are at least half an order of magnitude lower in amplitude than the dominant mode, and tend to lie outside of LIGO's sensitive frequency band for low-mass systems. Constrained by this strain sensitivity, we aim to determine the range of BBH mass, spin, and orbital orientations which maximizes the ratio of SNR for templates with and without HOMs. We will then calculate the maximum effective luminosity distance to the source, thus finding the optimal likelihood of detecting HOMs and paving the way for a powerful test of GR in the strong-field highly dynamical regime.

Usage: Caltech SURF Interim Report II.

I. INTRODUCTION

Gravitational waves (GWs) are violent ripples of spacetime created by catastrophic events such as colliding black holes, supernovae, and merging neutron stars. Predicted by physicist Albert Einstein in his Theory of General Relativity (GR) in 1915, Einstein's field equations show that such massive accelerating objects cause distorted waves to travel through the fabric of spacetime at the speed of light [1, 2].

Despite this breakthrough, GWs were not detected for another century, until September 14th, 2015, when the two detectors of the Advanced Laser Interferometer Gravitational-Wave Observatory (aLIGO) both observed the first GW signal, GW150914, at exactly 09:50:45.4 UTC [3]. Caused by a binary black hole (BBH) merger, GW150914 was detected during the first observing run (O1) of Advanced LIGO, which ran from September 12th, 2015 to January 19th, 2016 [4]. The second observing run (O2) ran from November 30th, 2016 to August 25th, 2017, and on August 1st, 2017, the Advanced Virgo detector joined O2, allowing for three detectors to simultaneously search for GWs for the first time in history [5].

This makes aLIGO the world's largest, most complex, and most sensitive interferometer, designed purely for the detection of these miniscule oscillations in spacetime. Soon, a global network of detectors will join aLIGO, with three detectors having already been built in Japan, Italy, and Germany [6], and a third LIGO detector to be built in India. Furthermore, the third observing run (O3) of Advanced LIGO and Virgo began in April 2019, and is planned to continue throughout the summer of 2019 for one calender year [7]. As such, gravitational waves are ushering in a new era of multi-messenger astronomy, in which astrophysicists have an entirely new way of viewing and understanding the cosmos.

A. Detection of Gravitational Waves

These developments represent an exciting opportunity to take advantage of the increased number of detections and enhanced signal-to-noise ratio (SNR), both of which will presumably only increase as the years go by. The implications of these improvements are numerous, as GWs carry not just energy and momentum, but crucial information about the structure of their sources. In partic-

* mshiferaw@college.harvard.edu
† ajw@caltech.edu
‡ lxxiao@caltech.edu

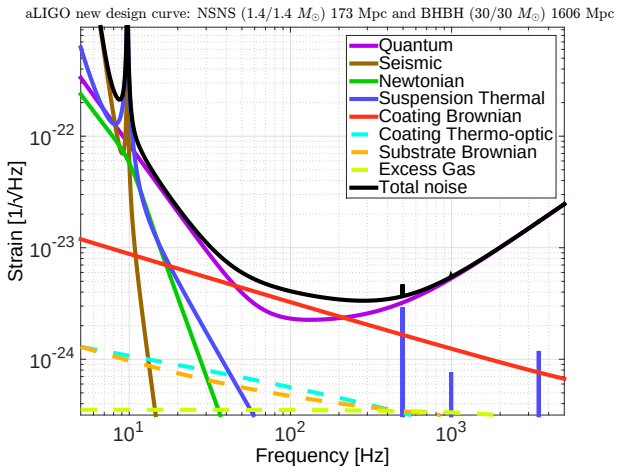

FIG. 1. The updated aLIGO design curve, which takes into account coating thermal noise. In black is the total noise of the design curve. Figure courtesy of LIGO Scientific Collaboration.

ular, a quasi-circular coalescing compact binary is completely characterized by fifteen parameters, which include the mass of each object in the merger, their spins, and their orbital orientation [8].

During an observing run, aLIGO continually takes in data, which means that these data must simultaneously be scrutinized for possible GW events. Events are thus detected using a technique called matched filtering, which selects the optimal model waveform for an observed signal from a *template bank*. Because the key parameters which describe a waveform, such as the amplitude, masses, spins, fiducial reference time, and orbital phase, are not known before matched filtering begins, such template banks search through parameter space to construct thousands of possible gravitational waveforms [9].

Matched filtering thus searches the data for resemblance to each template, for each time step dt of data. If a time step has an SNR $\gtrsim 8$, further investigations are done using Bayesian inference, a process which takes the model waveform and, given a range of parameters and expectations for noise, produces posterior distributions on the input parameters. With this, refined parameters can be extracted from any signal with a high enough SNR.

B. Higher Order Modes

During matched filtering, current model waveforms are restricted so that they only include the leading order Y_{22} mode of the waveform. This is because the full waveform, which includes the sum of all modes, depends on the viewing angle of the observer, something that is not known at the time of the search. This restriction, while providing reasonable estimations at a far less computationally expensive rate, comes at a cost: as both Payne et al. and Kumar et al. have shown, including HOMs provides tighter constraints on the source parameters than the fundamental $l = 2$ mode [10, 11].

This has three main benefits: including HOMs in our calculations will allow this parameter estimation procedure to become much more precise, thus greatly furthering our understanding of these GW sources. Furthermore, using waveforms with HOMs will likely increase the similarities between template and data during matched filtering, thus boosting aLIGO's detection confidence. Finally, including HOMs makes it possible to test for their presence in the signal found in the data, a powerful test of GR as the theory of strong gravity and GWs.

Unfortunately, there is yet another difficulty in including these HOMs in the parameter estimation process. HOMs are at least half an order of magnitude fainter than the dominant Y_{22} mode, and for low-mass systems, tend to lie outside of the total noise curve in aLIGO's sensitivity frequency band, depicted in Figure 1. This has a two-fold effect in both parameter estimation and matched filtering: this means that no HOMs have been detected yet, and will likely not be detected until either aLIGO's sensitivies improve or a detector happens to observe a close-by event with high SNR. As a result, in this project we aim to determine exactly how high in SNR an event detection needs to be in order to present statistically significant evidence for HOMs. In assessing the full extent of aLIGO's capabilities for detecting these HOMs, we will be able to better inform future detections, especially as aLIGO continues to be upgraded.

We will accomplish this by first computing the ratio of SNR for templates with and without HOMs. We will do so using BBH waveforms from the Simulating eXtreme Spacetimes (SXS) newly-released template bank, which includes HOMs as well as the dominant mode [12]. We will maximize this ratio for a range of input parameters, allowing us to determine optimal range of source merger mass, spin, and orbital orientation for detecting HOMs as constrained by aLIGO's total noise. Finally, we will calculate the maximum effective luminosity distance to the source which will allow aLIGO to detect this difference in SNR. Because HOMs are predicted by GR but have not yet been detected, this will also allow us to perform unique and powerful tests on GR in the strong-field, highly dynamical regime.

II. RELEVANT EQUATIONS

In this section, we outline relevant equations for the dominant Y_{22} mode of a gravitational waveform during the inspiral phase. The characteristic dimensionless gravitational wave strain amplitude h for a source of mass M located at a distance r away can be described by Equation 1. In this notation, Q refers to the quadrupole moment of the source event, ω is its angular frequency of oscillation, μ is the reduced mass, a is the separation between the two source frame component masses m_1 and

m_2, and M is the total mass of the merger [13]:

$$h \sim \frac{G}{c^4}\frac{1}{r}\frac{d^2Q}{dt^2}, \quad \frac{d^2Q}{dt^2} = -\omega^2 \mu a^2, \quad \mu = \frac{m_1 m_2}{M} = \frac{m_1 m_2}{m_1 + m_2} \tag{1}$$

The angular frequency ω can be rewritten in terms of the orbital period, using Kepler's third law in Equation 2:

$$\omega = 2\pi f_{\rm orb} = \frac{2\pi}{\tau_{\rm orb}}, \quad {\tau_{\rm orb}}^2 = \frac{4\pi^2}{G(m_1+m_2)}a^3 = \frac{4\pi^2}{GM}a^3 \tag{2}$$

Here, $f_{\rm GW} = 2f_{\rm orb}$, where $f_{\rm GW}$ refers to the frequency of the gravitational wave and $f_{\rm orb}$ is the orbital frequency. Equation 1 can thus be rewritten as Equation 3, where $R_{\rm S}$ is the Schwarzschild radius of the source and η is a unitless mass factor:

$$h \sim -\frac{GM}{c^2 r}\frac{G\mu}{c^2 a} \sim -\frac{\eta {R_{\rm S}}^2}{4ra} \tag{3a}$$

$$\eta = \frac{\mu}{M} = \frac{m_1 m_2}{M^2}, \quad R_{\rm S} = \frac{2GM}{c^2} \tag{3b}$$

The strain amplitude in Equation 3a can also be written in terms of the chirp mass $\mathcal{M}$, as defined by Equation 4 below:

$$h(t) \sim -\frac{1}{c^4 r}(G^5 \mathcal{M}^5 \pi^2 f_{\rm GW}^2(t))^{1/3}, \quad \mathcal{M} = M\,\eta^{3/5} \tag{4}$$

From these equations, it is clear that GWs can inform us about many features of the source event. Source parameters from newly detected GWs can thus be extracted using Bayesian parameter estimation, a method of mathematical modeling which is used to model real phenomena. In contrast to the classical frequentist approach, which chooses a value for some input parameter θ that maximizes the likelihood of the observed data, Bayesian parameter estimation holds the observed evidence as fixed and instead infers a Posterior Density Function (PDF) for θ [14]. Bayesian inference is a crucial tool in all of modern science, but is particularly useful in gravitational wave astronomy: a black hole can be completely characterized by its mass and spin vector, and the gravitational waveform from a BBH by a total of fifteen parameters [15]. These are composed of the following intrinsic parameters:

(1) the source frame component masses m_1 and m_2

(2) the source frame component spin vectors $\vec{\chi}_1$ and $\vec{\chi}_2$,

as well as the following extrinsic parameters:

(3) the luminosity distance d_L

(4) the source's sky localization $\Delta\Omega$, characterized by its right ascension (RA) and right declination (Dec)

(5) the polar angle ι and polarization angle ψ of the orientation of the binary orbit with respect to the line-of-sight of the observer

(6) the coalescence time t_c at which the signal from the merger reaches the center of the Earth

(7) the phase of the signal ϕ_c at the moment of coalescence

The observer's viewing angle to the source ι is a key parameter which differentiates the full waveform from the restricted waveform. For the latter, ι is indeed an extrinsic parameter, meaning that only the overall amplitude is dependent on it. In contrast, for the full waveform with HOMs, ι becomes an intrinsic parameter upon which the shape of the waveform is also dependent.

There are a number of other parameters which can be derived from these fifteen input parameters, including the final source frame mass M_f, the final spin a_f, the radiated energy $E_{\rm rad}$, the peak luminosity $l_{\rm peak}$, the redshift z, the chirp mass $\mathcal{M}$, and the dimensionless effective aligned spin $\chi_{\rm eff}$. The latter is described by Equation 5, where $\hat{L}_N$ is the Newtonian angular momentum of the source event:

$$\chi_{\rm eff} = \frac{(m_1\vec{\chi}_1 + m_2\vec{\chi}_2)\cdot\hat{L}_N}{M} \tag{5}$$

III. CURRENT PROGRESS

This project will require the use of SXS's newly-released template bank of waveforms with HOMs included, as well as the `GWpy` software package in Python [16]. Our approach consists of first visualizing a waveform for an example event with and without HOMs, and then generalizing to all events across many masses, spins and orbital inclinations in order to find the range of initial parameters that will maximize aLIGO's chances of detecting HOMs.

A. Visualizing the Waveform

In order to fully investigate HOMs, we must first gain a physical intuition for how the full waveform behaves compared to just the dominant mode, as well as individual HOMs. We do so through several plots and visualizations: in Figure 2, we establish that there is indeed a visible and quantitative difference between waveforms with HOMs and without HOMs. Here, as well as in Figures 3 and 4, we use the waveform for `SXS:BBH:0444`, a BBH merger with mass ratio 1.250 and orbital inclination 1.484×10^{-2}. In this image, the real amplitude of the strain is plotted for the dominant Y_{22} mode, as well as

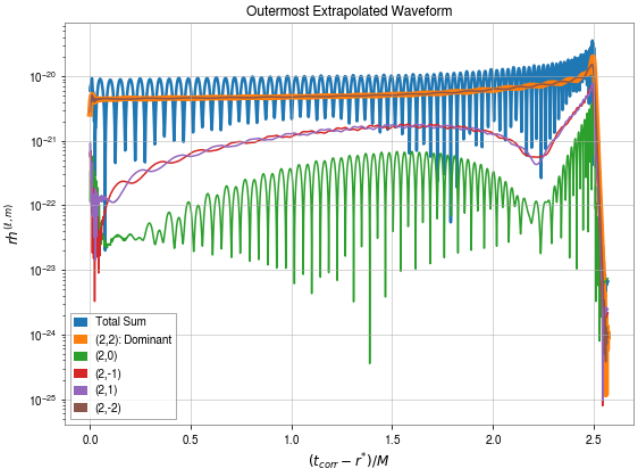

FIG. 2. The real strain amplitude of the fundamental Y_{22} mode for `SXS:BBH:0444`, along with four of the strongest HOMs. Despite this selection, the HOMs are at least half an order of magnitude weaker in amplitude than the dominant mode, and progressively become more and more noisy. Plotted in blue is the full waveform, or the total sum of all modes, which oscillates in time due to orbital precession. The merger is assumed to have a total mass of 100 $M_\odot$ at a distance 100 Mpc away.

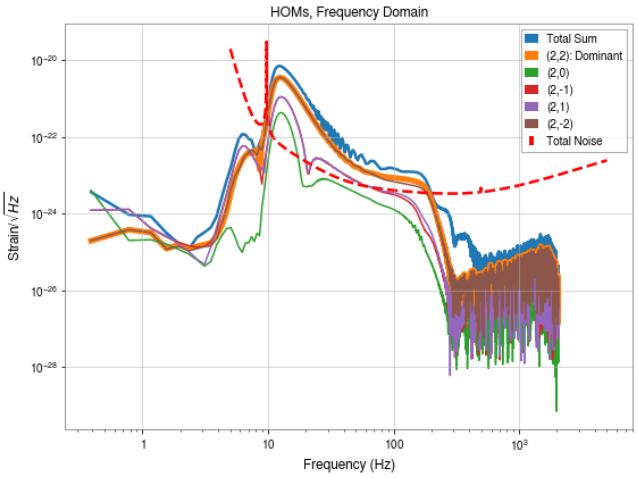

FIG. 3. The Fourier Transform of the interpolated simulation data for `SXS:BBH:0444`. In red is the LIGO design curve, and plotted in blue is the full waveform summing up all modes associated with this event. The merger is assumed to have a total mass of 100 $M_\odot$ at a distance 100 Mpc away.

four of the strongest HOMs. It is clear that the amplitude for the $Y_{2\pm1}$ mode is already half an order of magnitude smaller than the dominant mode, and subsequent HOMs tend to have increasingly weaker signals.

It should be noted that the beginning of each waveform in this figure, as well as in Figures 3 and 4, is exceedingly noisy. This is due to untrustworthy initial simulation data, and in the future this should be removed

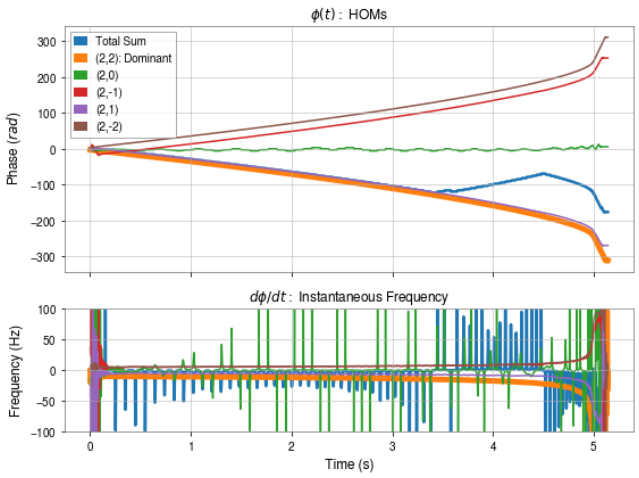

FIG. 4. The top panel depicts the phase of each mode of `SXS:BBH:0444`, as well as the full waveform. Opposite spherical harmonics monotonically increase in opposite directions, with $m = 0$ displaying little to no oscillations. The bottom panel plots the derivative of the phase, or the instantaneous frequency of each waveform. The frequency peaks, as expected, upon the time of coalescence. The merger is assumed to have a total mass of 100 $M_\odot$ at a distance 100 Mpc away.

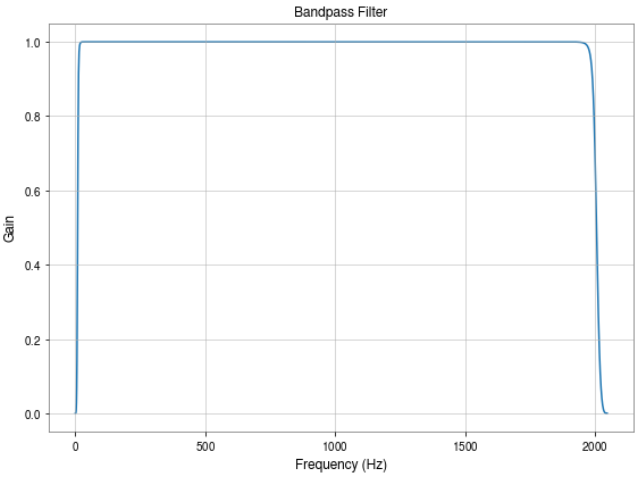

FIG. 5. The desired bandpass filter of 10-2000 Hz. This should filter out noisy simulation data from the beginning of the waveform.

from all plots. I am currently working on a way to automate this noise removal for all events and all modes by using a bandpass filter of 10-2000 Hz, as shown in Figure 5. Because we intend to focus on high-mass rather than low-mass systems, it is not expected that the frequency should ever exceed 2000 Hz.

Having visualized each of the modes in the time domain, we can now plot the HOMs as a function of frequency. Because the simulation data does not have a constant time-step, we must interpolate the waveform before performing a Fourier Transform. We do so at a sampling

rate of 4096 Hz, or twice the Nyquist frequency. After interpolation, we can plot the waveform for each mode, the dominant mode, and the sum of all modes against the total noise, obtained from aLIGO's updated design curve in Figure 1 (LIGO Scientific Collaboration). Doing so results in Figure 3, where the total noise serves as the Amplitude Spectral Density (ASD).

It should be noted that the excessive amount of noise visible in this plot at low frequencies $\lesssim 10$ Hz and high frequencies $\gtrsim 500$ Hz is not physical, but is instead due to Gibbs Noise. This is a phenomenon whereby the Fourier Transform of a piece-wise function results in a ringing artifact at the point of discontinuity. Because the SXS waveforms arbitrarily start at some time $t = 0$, the ringing artifact caused by this abrupt start becomes visible as high-frequency noise in the Fourier Transform. In contrast, the "humps" visible in the total sum at about 200-400 Hz are real effects of the underlying HOMs. As expected, there are clear differences between each of the HOMs, the dominant mode, and the full waveform.

Plotting these three curves together thus reveals the full range of frequencies in which the detectors can actually observe HOMs, as well as illustrating the delicate balance which exists between total merger mass, orbital orientation, and spin. A lower total mass increases the frequency of the merger and shifts the strain amplitude to the right, while the strain amplitude increases as the merger becomes more face-on. Adding spin will complicate this even further, as a merger might also precess about its orbital plane, and thus the observer's viewing angle with respect to the line of sight [17]. The effect of this precession on the observed waveform is better seen edge-on rather than face-on, but strain amplitudes are highest for face-on systems.

Finally, we plot the waveform peak frequency as a function of time, as depicted in Figure 4. Plotted in the top panel is the phase for each mode, as well as the full waveform, and in the bottom panel is the instantaneous frequency. The phase appears to monotonically increase in opposite directions for opposite spherical harmonics, aside from the $m = 0$ modes, which appear to have little to no oscillations. The instantaneous frequency fluctuates very heavily in the beginning due to noisy data, stabilizes for the most part, and then fluctuates heavily until it reaches peak frequency during coalescence. The maximum peak frequency for any individual mode of `SXS:BBH:0444` at a total mass of 100 $M_\odot$ is less than 2000 Hz.

B. Computing the Overlap Integral

Now that we are able to visualize the waveform with and without HOMs, we compute the optimal SNR as a function of total merger mass, mass ratio, spin, and orbital orientation angle with respect to the observer's line of sight. More quantitatively, we compute the overlap integral $\mathcal{O}$ between the dominant Y_{22} mode and waveform with HOMs in order to find where the overlap is smallest. Because an overlap integral is essentially an inner product, if h_1 and h_2 are identical, then $\mathcal{O}$ will be equal to 1. The less they have in common, the smaller $\mathcal{O}$ is, indicating that the full signal with HOMs will be distinguishable from the dominant mode. The overlap integral is shown in Equation 6 below, where $h_1(f)$ and $h_2(f)$ are the waveform with and without HOMs, and PSD is the Power Spectral Density, referring to the square of the total design noise curve depicted in Figure 1:

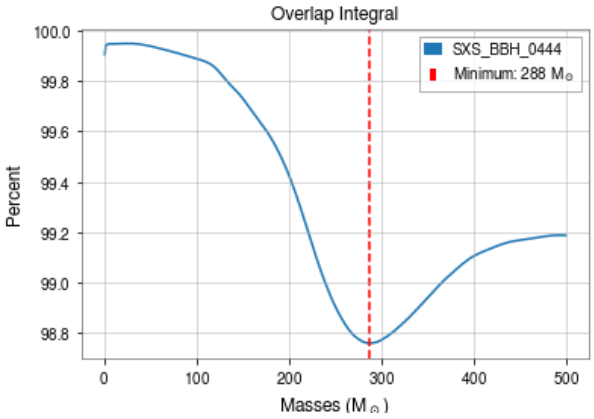

FIG. 6. The overlap integral computed for a range of masses 1 to 500 $M_\odot$. The overlap appears to reach a minimum for mergers with a total mass 280 $M_\odot$, signifying that HOMs may be able to be distinguished from the dominant waveform.

$$\mathrm{PSD} = \mathrm{ASD}^2 \tag{6a}$$

$$\langle h_1|h_2\rangle = \int df \frac{h_1(f)\, h_2^*(f)}{\mathrm{PSD}(f)} \tag{6b}$$

$$\mathcal{O} = \frac{\langle h_1|h_2\rangle}{\sqrt{\langle h_1|h_1\rangle\langle h_2|h_2\rangle}} \tag{6c}$$

Performing this integral for `SXS:BBH:0444` with a range of masses 1 to 500 $M_\odot$ produces the plot depicted in Figure 6. There is a clear dip in the overlap integral at 280 $M_\odot$, signifying that this is the total merger mass which optimizes the likelihood of detection of HOMs in the waveform of `SXS:BBH:0444`. Moving forward, we must repeat this process for all promising events with a long enough duration at high masses, at a range of orbital inclinations and spins. We will also need to revisit the way in which we compute the overlap integral: currently, each overlap integral is determined at a range of frequencies specific to each mode and each event. In order to standardize this calculation, we will need to decide a standard frequency range over which to integrate and simply zero-pad any gaps in the data.

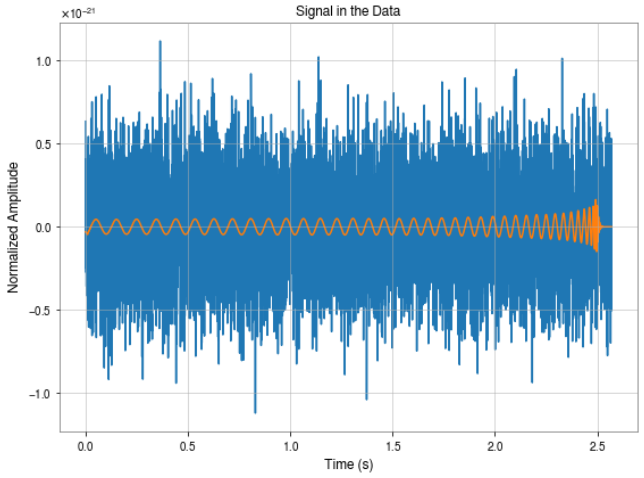

FIG. 7. An example of a full gravitational waveform signal, plotted in orange, hidden in noisy data, plotted in blue. This signal uses simulation data from `SXS:BBH:0444`, assuming a total mass of 100 $M_\odot$ at a distance 20 Gpc away.

This overlap integral will inform us as to which HOMs are statistically significant and which are negligible. Experimenting with different masses and spins will also visually guide us to which combination is optimal, allowing us to gain an intuition for the SNR. However, it is important to note that the total noise curve depicted in Figure 1 is an idealization of the noise curve. Noise, by definition, is random in time, but because the PSD is an average of many noise realizations, it is constant in the frequency domain. In order to find the optimal range of parameters in a more realistic fashion, we will need to work in the time domain of the noise. An example of what aLIGO's data might look like is illustrated in Figure 7, where the full GW signal is visibly buried in the noise.

IV. CHALLENGES

One of the biggest challenges thus far has been in starting my new project from scratch two weeks into the program. As a result, I anticipate that it will be difficult to complete all of our goals in time before the program ends. Other challenges I have encountered mainly involved getting acquainted with technical methods, such as downloading the appropriate software, learning how to perform a Fourier Transform on a simulated waveform from the SXS catalogue, and figuring out how to convert the units in the ASD from strain to strain/$\sqrt{(Hz)}$. Lastly, I found it difficult to derive certain conceptual terms, such as expression for frequency in terms of time, the Innermost Stable Circular Orbit (ISCO) radius, and frequency at ISCO.

Currently, my biggest challenges center around refining certain aspects of my project: I am having difficulty figuring out a consistent, reliable, and efficient way to remove the noise from the initial simulation data. I am also finding it challenging to adapt the overlap integral calculation to a constant range, rather than modifying it for each specific scenario, as I have been doing thus far. Lastly, I am still attempting to learn how to download the waveform data for each event, which contains information for hundreds of masses, in a reliable way, ideally in an `HDF` file.

Once I have overcome these obstacles, I anticipate that the most challenging parts of my project will revolve around adjusting my code to iterate over a range of spins and orbital inclinations, as well as learning to understand quaternions.

ACKNOWLEDGEMENTS

I would like to thank Alan Weinstein for serving as my research advisor on this project, as well as Jonah Kanner and Liting Xiao for their guidance. I would also like to thank the Caltech Student Faculty Program (SFP) for organizing the LIGO SURF program. Finally, I would like to thank the National Science Foundation (NSF) for their funding.

[1] Einstein A. Approximative Integration of the Field Equations of Gravitation. Sitzungsber Preuss Akad Wiss Berlin (Math Phys). 1916;1916:688–696.
[2] Einstein A. ber Gravitationswellen. Sitzungsber Preuss Akad Wiss Berlin (Math Phys). 1918;1918:154–167.
[3] Abbott BP, Abbott R, Abbott TD, Abernathy MR, Acernese F, Ackley K, et al. Observation of Gravitational Waves from a Binary Black Hole Merger. Phys Rev Lett. 2016 Feb;116:061102. Available from: https://link.aps.org/doi/10.1103/PhysRevLett.116.061102.
[4] The LIGO Scientific Collaboration, the Virgo Collaboration, Abbott BP, Abbott R, Abbott TD, Abraham S, et al. GWTC-1: A Gravitational-Wave Transient Catalog of Compact Binary Mergers Observed by LIGO and Virgo during the First and Second Observing Runs. arXiv e-prints. 2018 Nov;p. arXiv:1811.12907.
[5] Acernese F, Agathos M, Agatsuma K, Aisa D, Allemandou N, Allocca A, et al. Advanced Virgo: a second-generation interferometric gravitational wave detector. Classical and Quantum Gravity. 2015 Jan;32(2):024001.
[6] Abbott BP, Abbott R, Adhikari R, Ajith P, Allen B, Allen G, et al. LIGO: the Laser Interferometer Gravitational-Wave Observatory. Reports on Progress in Physics. 2009 Jul;72(7):076901.

[7] Turpin D, Wu C, Han XH, Xin LP, Antier S, Leroy N, et al. The mini-GWAC optical follow-up of the gravitational wave alerts: results from the O2 campaign and prospects for the upcoming O3 run. arXiv e-prints. 2019 Feb;p. arXiv:1902.08476.

[8] Cai RG, Cao Z, Guo ZK, Wang SJ, Yang T. The Gravitational-Wave Physics. arXiv e-prints. 2017 Mar;p. arXiv:1703.00187.

[9] Babak S, Balasubramanian R, Churches D, Cokelaer T, Sathyaprakash BS. A template bank to search for gravitational waves from inspiralling compact binaries: I. Physical models. Classical and Quantum Gravity. 2006 Sep;23(18):5477–5504.

[10] Payne E, Talbot C, Thrane E. Higher order gravitational-wave modes with likelihood reweighting. arXiv e-prints. 2019 May;p. arXiv:1905.05477.

[11] Kumar P, Blackman J, Field SE, Scheel M, Galley CR, Boyle M, et al. Constraining the parameters of GW150914 and GW170104 with numerical relativity surrogates. Phys. Rev. D. 2019 Jun;99(12):124005.

[12] Boyle M, Hemberger D, Iozzo DAB, Lovelace G, Ossokine S, Pfeiffer HP, et al. The SXS Collaboration catalog of binary black hole simulations. arXiv e-prints. 2019 Apr;p. arXiv:1904.04831.

[13] Centrella JM. What can we learn about cosmic structure from gravitational waves? In: Holt SH, Reynolds CS, editors. The Emergence of Cosmic Structure. vol. 666 of American Institute of Physics Conference Series; 2003. p. 337–346.

[14] Eshky A. Bayesian Methods of Parameter Estimation Aciel Eshky; 2009. .

[15] Thrane E, Talbot C. An introduction to Bayesian inference in gravitational-wave astronomy: Parameter estimation, model selection, and hierarchical models. . 2019 Mar;36:e010.

[16] Macleod D, Urban AL, Coughlin S, Massinger T, paulaltin, Areeda J, et al.. gwpy/gwpy: 0.14.2; 2019. Available from: https://doi.org/10.5281/zenodo.2603187.

[17] Dietrich T, Bernuzzi S, Brügmann B, Ujevic M, Tichy W. Numerical relativity simulations of precessing binary neutron star mergers. Phys. Rev. D. 2018 Mar;97(6):064002.